Beneficial Effect of a Pre-ceramic Polymer Coating on the Protection at 900 °C of a Commercial AISI 304 Stainless Steel

Frédéric Riffard, Eva Joannet, Henri Buscail, Raphaël Rolland, Sébastien Perrier

Beneficial Effect of a Pre-ceramic Polymer Coating on the Protection at 900 °C of a Commercial AISI 304 Stainless Steel

Frédéric Riffard, Eva Joannet, Henri Buscail, Raphaël Rolland, Sébastien Perrier

LVEEM, E.A. 3864, Clermont-Université-UdA, I.U.T. Département Chimie Sciences des Matériaux, 8 rue J.B. Fabre, CS 10219, 43009 Le Puy-en-Velay Cedex, France.

frederic.riffard@udamail.fr; eva.joannet@gmail.com; henri.buscail@udamail.fr; raph43@hotmail.fr; sebastien.perrier@udamail.fr

Abstract. An effective and low-cost method for applying polysilazane-based barrier coating on stainless steel is presented. A SiN (PHPS) precursor has been used for applications of polymeric and ceramic-like coating material. With precursor solution in dibutyl ether, AISI 304 stainless steel substrates were coated by means of a simple dip coating technique. After pyrolysis stage at 800 °C, the efficiency of the PHPS-based coating has been proved, and oxidation tests were done at 900 °C in air. By measuring the weight gain, and by using analytical techniques as *in situ* X-Ray Diffraction and Scanning Electron Microscopy, it has been shown that an amorphous silica layer formed from the initial PHPS-based coating and acts as a protective glass which provides complete separation of the AISI 304 steel surface from the oxidizing environment. This protective silica layer appears to be a very good diffusion barrier by preventing iron-containing oxide formation.

Keywords: High temperature oxidation, AISI 304 steel, Silicon, Pre-polymer ceramic coating, *in situ* X-Ray Diffraction

INTRODUCTION

Silica coatings are potential candidates for improving the resistance against high temperature corrosion of metals [1-3]. Various techniques had been used to prepare silica coatings, such as vacuum deposition [4], sputtering, chemical vapour deposition (CVD) [5], or sol-gel [6, 7] methods. However, the drawbacks of these techniques, such as high cost (complex and expensive instruments for vacuum deposition, CVD) have limited their application in industry.

In recent years, another alternative, low-cost and feasible route, has garnered interest for generating silica coatings which is mainly based on the use of silicon containing precursors like polysiloxanes [8, 9], polycarbosilanes [10], polysilazane [11-14], because most of the precursors are liquids or solids that can be dissolved in many organic solvents, such as benzene, toluene, xylene, pyridine, … that allows to use more simple processing techniques, e.g. dip- or spin- coating [15].

Basically, these pre-ceramic polymers are thermoset-materials containing a comparably short chain molecule that have been rearranged into a highly bonded rigid network during subsequent cross-linking process and lose of their organic components to form an amorphous or nanostructured ceramic upon pyrolysis at higher temperature [15]. The pyrolysis stage is called the "polymer-to-ceramic conversion" which is the crucial step for the resulting polymer-derived ceramics' structures and properties.

The aim of this work is to develop a polymer derived ceramic coating on a commercial AISI 304 stainless steel as a barrier to oxidation at high temperature. Perhydropolysilazane (PHPS) provided by the Clariant Company, was used as a pre-ceramic polymer and deposited on the steel substrate using dip-coating method.

In this work, we report the influence of the pyrolysis in air on the investigated films based on PHPS, and on the oxidation protection effect of precursor-coating on the AISI 304 steel substrates by the measurements of weight gain, *in situ* X-Ray Diffraction (XRD) and Scanning Electron Microscopy (SEM).

EXPERIMENTAL PROCEDURES

The substrate material chosen in the present study is a commercial AISI 304 stainless steel which chemical composition is given on table 1.

The substrate coupons are obtained from a steel rolled plate with a 2 mm thickness, and are shaped to the dimensions 10 x 20 mm^2 for oxidation tests. A 1.8 mm diameter hole is bored into the coupons to hang the samples during the different experimental steps (dip-coating, pyrolysis treatment and oxidation tests).

The steel specimen surfaces are mechanically polished with SiC paper up to the 800 grade, and then cleaned in ethanol, rinsed with distilled water and finally dried in air.

TABLE 1. Chemical composition of the steel substrate (weight %) obtained by ICPMS

Alloy 304	Fe	Cr	Ni	Mn	Si	Co	Mo	Cu	C
wt. %	Bal.	17.90	9.05	1.52	0.48	0.22	0.15	0.10	0.05

After this initial preparation, the specimens are immediately coated with PHPS precursor by means of dip-coating. The coated samples are dried in laboratory air for 24 hours at room temperature prior to other operations.

The precursor has been provided by Clariant as a dibutyl ether solution of perhydropolysilazane (20 weight % polysilazane NN 120-20, Clariant Corp. Germany). PHPS is produced by ammonolysis of the dichlorosilane, SIH_2Cl_2 [16]. The PHPS unit structure contains a huge amount of Si-N-H groups (Figure 1) which can easily react with hydroxyl groups [17].

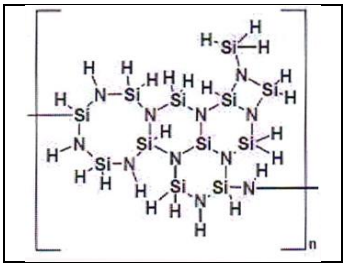

FIGURE 1. Basic structure of the PHPS precursor

Actually, under normal conditions, there are adsorbed hydroxyl groups on the surface of the steel substrate before dip-coating. So PHPS reacts with these adsorbed hydroxyl groups [18] to form generate metal-O-Si chemical bonds between the steel substrate and the PHPS-based coating which contribute to the coating adhesion.

The as-formed pre-ceramic polymers are generally of low molecular weight which gives a very low ceramic yield upon pyrolysis. Cross-linking of the oligomer precursor compounds into large molecules with highly interlocked backbones is needed to avoid the evaporation of oligomers during pyrolysis [19]. In the present study, a first heat treatment of the as-coated samples is performed at 200 °C for one hour under laboratory air in order to ensure the cross-linking of the coating.

After the cross-linking heat treatment, the coating is pyrolized at higher temperature. The pyrolysis temperature has been fixed at 800 °C in air, and the pyrolysis duration has been fixed at 1 hour.

The isothermal weight gain measurements at 900 °C were carried out by thermogravimetry (TGA) using a TG-DTA 92-1600 Setaram microthermobalance during about 90 h in order to follow the oxidation kinetic.

Characterization of the oxide scale was carried out by *in situ* X-ray diffraction. *In situ* X-ray diffraction analyses were carried out during the first 24 h oxidation by means of a high temperature MRI chamber in a Philips X'pert MPD diffractometer. The diffractometer goniometer is equipped with a curved Cu monochromator to cut off the diffracted CuK_α wavelength from all other wavelengths such as iron fluorescence radiation. *In situ* XRD analysis were performed using Cu $K_{\alpha 1}$ radiation, λ = 0.15406 nm. X-ray patterns were registered every hour to follow the

main compounds evolution during the high temperature oxidation tests. Only the most representative patterns will be presented in our study.

After cooling, the oxide scale surface and cross-section morphologies have been observed in a JEOL 6400 scanning electron microscope (SEM) coupled with a LINK energy dispersive X-ray spectroscopy (EDXS). The EDXS point analyses were performed with an electron probe focused to a 1µm spot.

EXPERIMENTAL RESULTS

The efficiency of the PHPS-based coating against isothermal high temperature oxidation has been tested by the thermogravimetry method in air at 900 °C. Figure 2 gives the weight gain curves obtained after 90-h oxidation of PHPS-coated and uncoated AISI 304 steel specimens.

The weight gain curve recorded on blank AISI 304 clearly exhibits an initial transient linear regime during the first 20-h oxidation test ("transient" stage). After 20 h, Figure 2 reveals that a breakaway oxidation process occurs, and the weight gain after 90-h oxidation is about 2.22 mg/cm^2.

PHPS-coated samples follow a predominant linear regime all along the oxidation test, since chromium diffusion takes place in a silica layer of a constant thickness, and the weight gain after 90-h oxidation is only about 0.10 mg/cm^2. These experimental results underline the beneficial effect of the PHPS-based coating, which allows to inhibit the initial transient stage and to reduce significantly the weight mass gain registered at the end of the oxidation test by a factor of about 20.

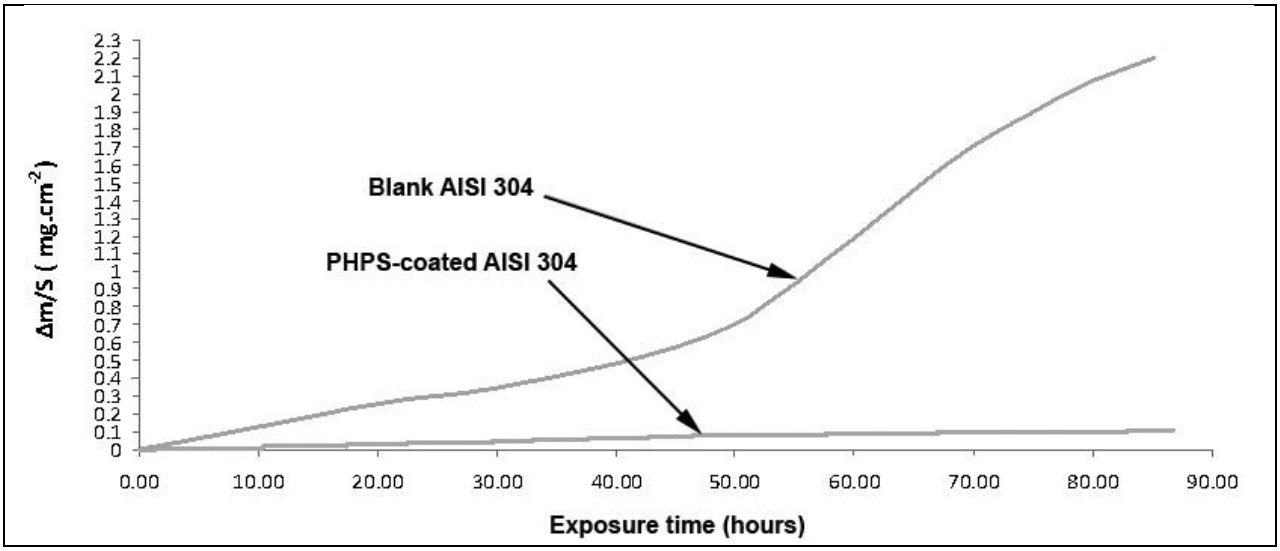

FIGURE 2**.** Weight gain curves obtained on blank and PHPS-coated 304 stainless steel specimens at 900 °C in air.

Figure 3 shows the *in situ* XRD patterns obtained on the blank AISI 304 specimen oxidised during the first 24 hours. The crystalline compounds present in the oxide scale are identified as Cr_2O_3 chromia (ICDD 38-1479) and a spinel type oxide: $Mn_{1.5}Cr_{1.5}O_4$ (ICDD 33-0892).

At the beginning of the oxidation test, the successive patterns reveal the initial nucleation of Fe_2O_3 hematite (JCPDS 33-664), together with the other initial detected oxides. Fe_2O_3 is observed up to the end of the oxidation test, as well as the metallic structure of the stainless steel (γ-austenite (ICDD 33-0397)).

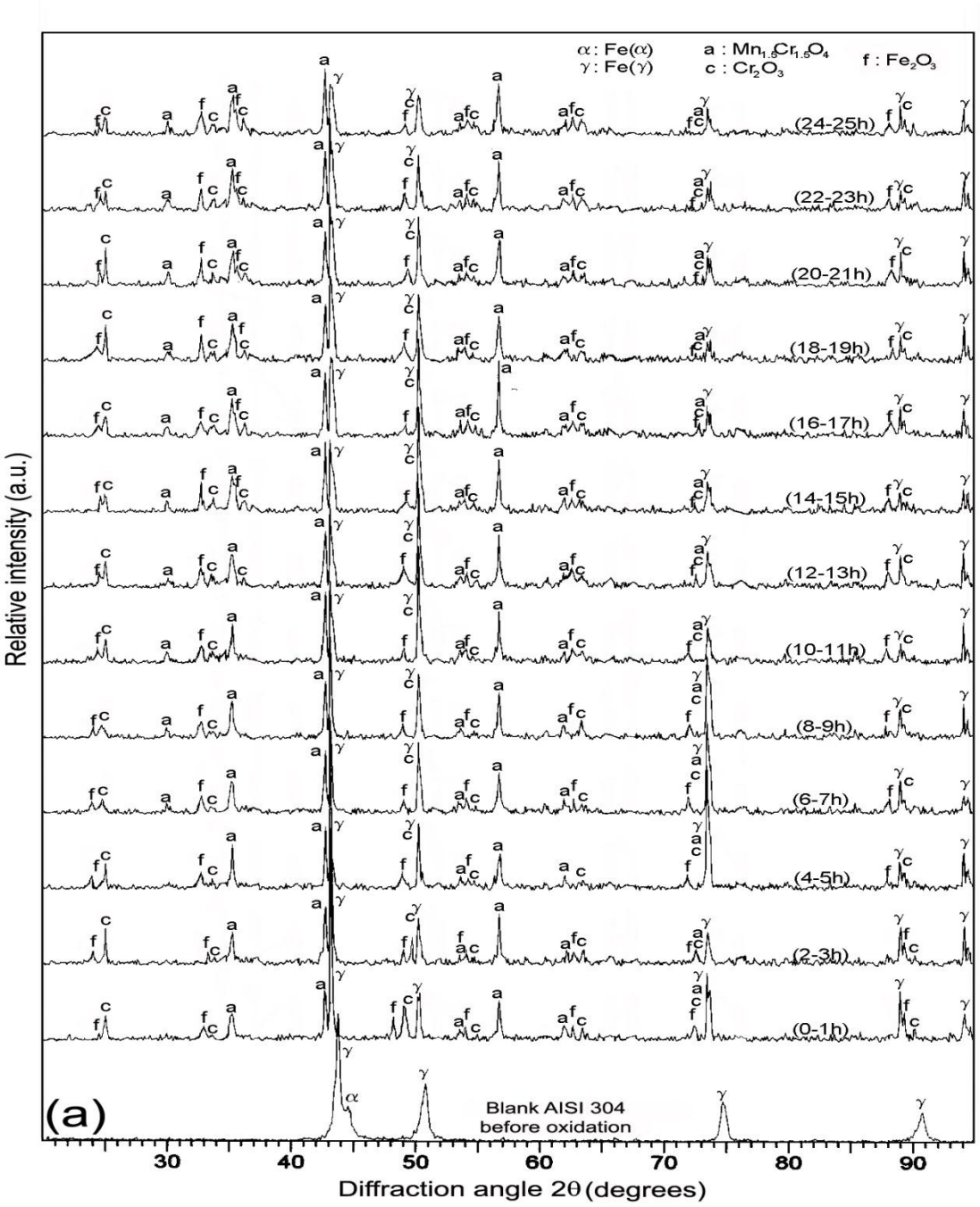

FIGURE 3. *In situ* XRD patterns registered at 900 °C for 24h in air on blank AISI 304 specimen.

Figure 4 shows the *in situ* XRD patterns obtained on the PHPS-coated AISI 304 specimen oxidised during the first 48 hours of isothermal treatment. The high relative intensity of the alloy diffraction peaks during the whole experiment suggests that the PHPS-coated specimen is very slowly oxidised. The initially formed oxides (e.g. Cr_2O_3 and $Mn_{1.5}Cr_{1.5}O_4$) were detected all along the oxidation test. By contrast, no iron oxides were detected on coated specimen. In addition, no diffraction peaks correlated to the PHPS-based coating was identified, which assumed the formation of an amorphous silica coating.

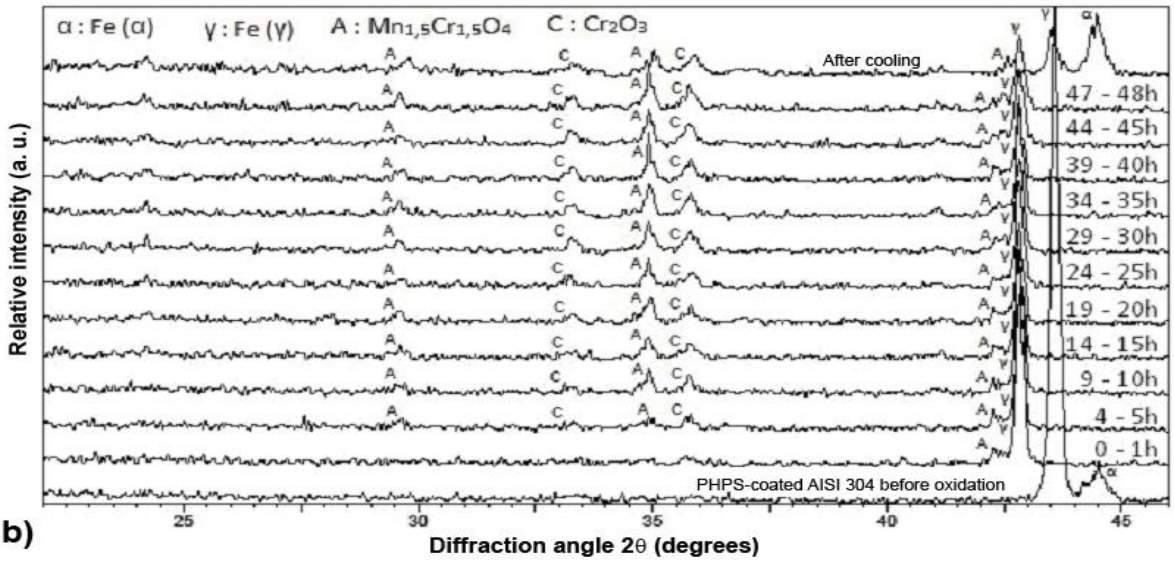

FIGURE 4. *In situ* XRD performed at 900 °C for 48 h in air on PHPS-coated AISI 304 specimen.

Figure 5 shows the specimen's surface scale morphologies (SEI images). Blank specimen oxidized during 24h is covered by a chromia scale and manganese chromite grains (Figure 5a). Spalled areas are found on about 50% of the blank specimen surface. The PHPS-based coating induces no scale spallation on the surface (Figure 5b). An amorphous silica layer is detected on the top of the steel surface, which is formed from the PHPS-based coating. A significant accumulation of manganese-containing spinel oxides is detected in damaged areas where the initial PHPS-based coating was found to be cracked (Figure 5b).

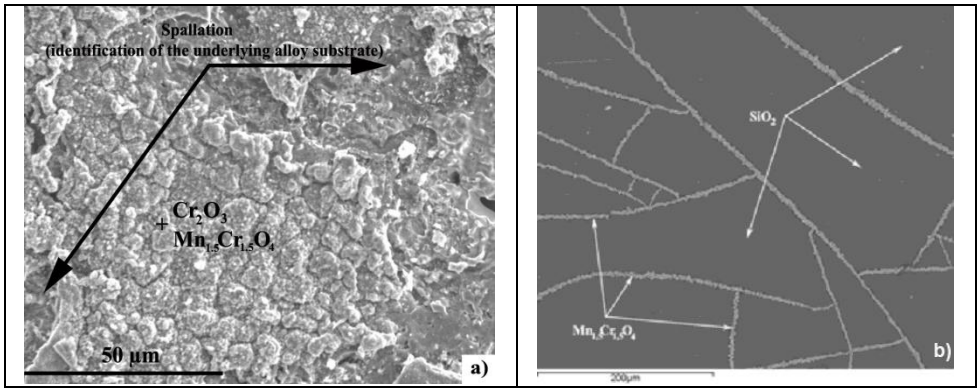

FIGURE 5. SEM surface micrographs of the specimens oxidized at 900 °C in air (SEI), effect of PHPS-based coating. a) Blank AISI 304 steel ; b) PHPS-coated AISI 304 steel .

The scale cross-section morphologies are presented on Figure 6. Blank specimen oxidized during 24 h shows an internal adherent subscale of about 5 µm thick, mainly composed of Cr_2O_3 chromia and $Mn_{1.5}Cr_{1.5}O_4$ manganese chromite. SiO_2 silica is found at the internal interface (figure 6a). On the PHPS-coated AISI 304 steel, no scale spallation is observed on the cross-section (Figure 6b). The oxide scale is 1 µm thick, mainly composed of an amorphous and continuous silica layer formed from the initial PHPS-based coating. Cr_2O_3 chromia is detected on the top of the coating and manganese chromite enrichment is identified in damaged areas where the silica layer was not continuous (Figure 6b).

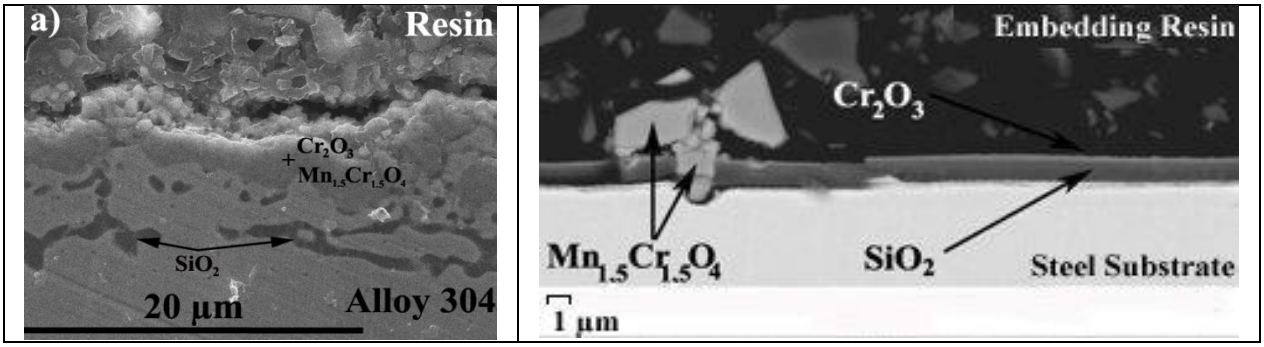

FIGURE 6**.** SEM cross-section micrographs of the specimens oxidized at 900 °C in air (BSE), effect of PHPS-based coating. a) Blank AISI 304 steel; b) PHPS-coated AISI 304 steel.

EDS analysis (Figure 7) of the PHPS-coated AISI 304 steel clearly shows a combined accumulation of Si and O elements on top of the steel, which implies an amorphous silica layer formation from the PHPS-based coating. Chromium element appears to diffuse through this silica layer to form chromia layer on the top of the coating. Cr, Mn, O elements-enriched compounds are detected in areas where the silica layer is not continuous, which involves the manganese-containing spinel oxide formation where the initial PHPS-based coating was to be found cracked.

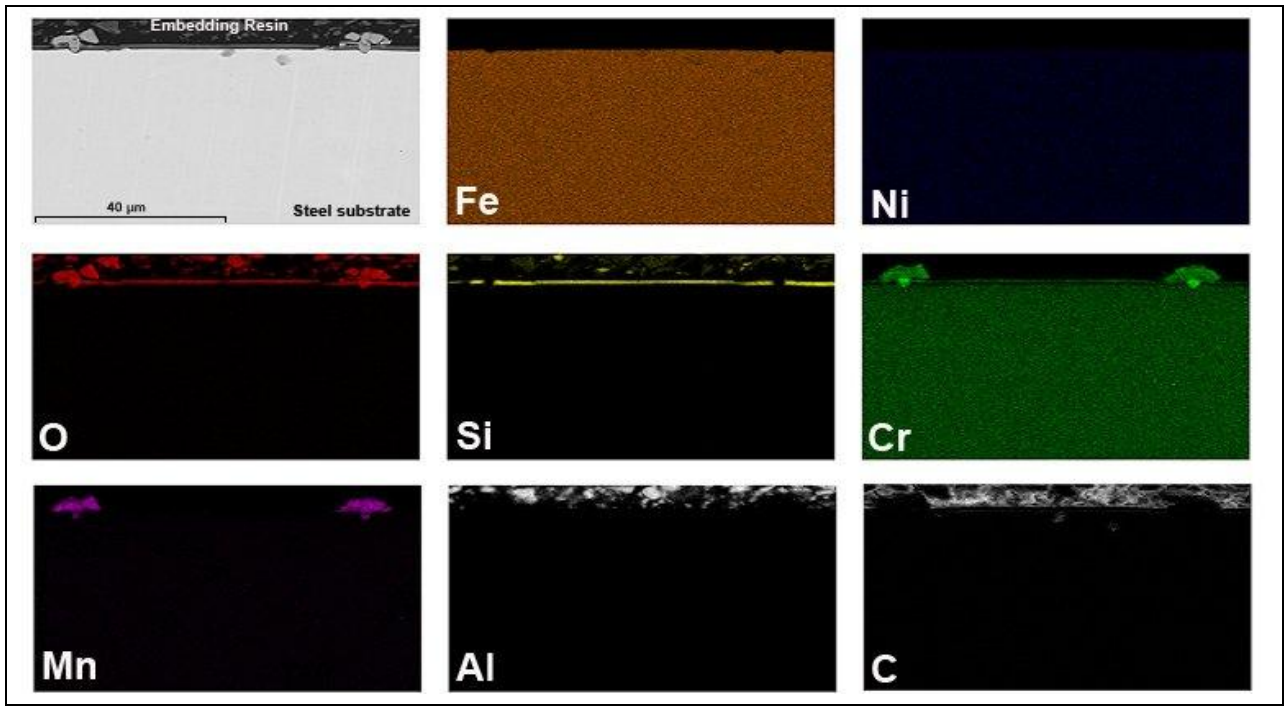

FIGURE 7**.** Element distribution (EDXS mapping) of the PHPS-coated AISI 304 steel oxidized at 900 °C for 48 h in air.

DISCUSSION

A predominant diffusion process controls the oxidation kinetic of the blank AISI 304 specimen, though a chemical process also occurs during the first 20-h oxidation test, leading to a very high mass gain per unit surface area during the first hour of isothermal oxidation. During this initial stage of oxidation, *in situ* XRD analyses reveal the formation of an oxide scale mainly composed of Cr_2O_3, $Mn_{1.5}Cr_{1.5}O_4$ and Fe_2O_3 (Figure 3). Especially at the particular temperature of 900 °C, a combination of linear and exponential rate laws is observed. The shape of the

mass gain curve versus oxidation time shows a "breakaway" after 20 hours of the oxidation test (Figure 2). This peculiar behaviour could be attributed to the initial and very fast Fe_2O_3-hematite growth.

Iron diffuses outwards and Fe_2O_3 is formed at the air/oxide interface. This process induces iron depletion at the scale/steel interface. Then, nickel becomes predominant and voids form at this interface. Voids coalescence induces the outer scale spallation observed when the specimen was cooled down to room temperature (Figure 5a).

Porous, and not very protective [20], the hematite formation leads to the initial establishment of a linear oxidation regime, and finally to a re-acceleration of the oxidation kinetic as a breakaway phenomenon occurring from 20 hours and up to the end of the oxidation test. Several mechanisms leading to oxide scale failure and to the breakaway phenomenon on stainless steel appear in the literature. They are generally classed into three groups: failure by scale volatilization [21-23], pure chemical failure [24], mechanically induced failure [24]. Intentional cracking by sample bending after a first oxidation period led to iron oxide growth along the cracks [25]. Through-scale cracking is therefore a main way to oxide scale failure. This generates diffusion paths for iron and its initial oxidation leads to the hematite formation and to the breakaway phenomenon.

Kinetic results have shown that the PHPS-based coating leads to a lower oxidation rate compared to blank specimen (Figure 2). On the PHPS-coated AISI 304 steel, the oxide scale protective character is confirmed by *in situ* XRD analysis (Figure 4) and SEM surface analyses (figure 5b), which show the chromia scale formation. It also exhibits the manganese chromite growth from the beginning of the oxidation process at 900 °C. No iron-containing oxides are detected by XRD or SEM analyses, and scale spallation has not been observed.

In situ XRD analysis (Figure 4) also shows that the PHPS-based coating is not crystalline after pyrolysis stage at 800 °C and before oxidation test. SEM micrographs (Figures 5b and 6b) show the formation of a continuous silica layer coming from the initial PHPS-based coating, as confirmed by the element distribution of the PHPS-coated AISI 304 steel after oxidation at 900 °C (Figure 7). After pyrolysis stage at 800 °C for 1 h in air, the initial PHPS-based coating reacts with oxygen leading to an amorphous silica layer [26] at the steel surface which acts as a diffusion barrier for the chemical diffusing species (especially iron and manganese) [27]. This amorphous silica layer acts as a protective glass which provides complete separation of the AISI 304 steel surface from the oxidizing environment. The protective character of the PHPS-based coating is also expressed by the very low oxidation rate (Figure 2), and by the high relative intensity of the alloy diffraction peaks observed during the *in situ* XRD analyses (Figure 4) which attest of a very low oxide thickness.

On the PHPS-coated AISI 304 steel, the oxide scale protective character is confirmed by *in situ* XRD analysis (Figure 4) which proves the efficiency of the PHPS-based coating [26, 28-31] by totally inhibiting the iron-containing oxide formation. XRD analysis (Figure 4) also shows the chromia scale formation, and SEM cross-section analyses (figure 5b) coupled with EDXS analyses (Figure 7) attest that this chromia scale grows on top of the initial silica layer coming from the PHPS-based coating. This means that silica layer acts as a diffusion barrier especially for iron, but not for chromium. XRD analysis (Figure 4) also exhibits the manganese chromite growth from the beginning of the oxidation process at 900 °C. SEM cross-section analyses (figure 5b) coupled with EDXS analyses (Figure 7) show that this manganese-containing spinel oxide is preferentially localized in areas where the initial PHPS-based coating was found to be cracked during cooling after pyrolysis stage at 800 °C for 1h in air.

CONCLUSIONS

The commercially available PHPS polysilazane precursor seems to be very suitable to protect alloys as AISI 304 stainless steel from oxidation. The PHPS-based coating can be applied by simple dip- and spray-techniques. Due to the high oxygen reactivity of the silazanes, direct chemical bonds between the coating and the substrate are formed, leading to good adhesion.

After thermal treatment occurring during the pyrolysis stage at 800 °C for 1 h in air, the initial PHPS-based coating reacts with oxygen leading to form an amorphous silica layer at the steel surface which acts as a diffusion barrier for the chemical diffusing species. This amorphous silica layer acts as a protective glass which provides complete separation of the AISI 304 steel surface from the oxidizing environment. This protective silica layer appears to be a very good diffusion barrier especially for iron, but not for chromium. By preventing iron-containing oxide formation, this PHPS-based coating proves its efficiency to protect AISI 304 steel substrates from oxidation at 900 °C in air.

REFERENCES

1. A. Pepe, M. Aparicio, A. Duran and S. Cere, *Journal of Sol-Gel Science and Technology*, **39**, 131 (2006).
2. S.J. Kim, M. Hara, R. Ichino, M. Ochido and N. Wada, *Materials Transactions*, **44**, 782 (2003).
3. J. De Damborenea, N. Pellegri, O. Sanctis and A. Duran, *Journal of Sol-Gel Science and Technology*, **4**, 239 (1995).
4. Y. Morisada, T. Sakurai and Y. Miyamoto, *International Journal of Applied Ceramic Technology*, **1**, 374 (2004).
5. B. Borer, A. Sonnenfeld and P.R. von Rohr, *Surface and Coating Technology*, **201**, 1757 (2006).
6. O. De Sanctis, L. Gomez, N. Pelligri and A. Duran, *Surface and Coating Technology*, **70**, 251 (1995).
7. Y. Castro, B. Ferrari, R. Moreno and A. Duran, *Surface and Coating Technology*, **182**,199 (2004).
8. O. Goerke, E. Feike, T. Heine, A. Trampert and H. Schubert, *Journal of European Ceramic Society*, **24**, 2141 (2004).
9. J.D. Torrey and R.K. Bordia, *Journal of European Ceramic Society*, **28**, 253 (2008).
10. P. Colombo, T.E. Paulson and C.G. Pantano, *Journal of American Ceramic Society*, **80**, 2333 (1997).
11. T. Kubo, E. Tadaoka and H. Kozuka, *Journal of Sol-Gel Science and Technology*, **31**, 257 (2004).
12. Y. Naganuma, S. Tanaka, C. Kato and T. Shindo, *Journal of Ceramic Society of Japan*, **112**, 599 (2004).
13. H. Kozuka, M. Fujita and S. Tamoto, *Journal of Sol-Gel Science and Technology*, **48**, 148 (2008).
14. E. Bernardo, P. Colombo and S. Hampshire, *Journal of European Ceramic Society*, **29**, 243 (2009).
15. E. Kroke, Y.L. Li, C. Konetschny, E. Lecomte, C. Fasel and R. Riedel, *Materials Science Engineering: R: Reports*, **26**, 97 (2000).
16. T. Isoda, H. Kaya, H. Nishii, O. Funayama, T. Suzuki and Y. Tashiro, *Journal of Inorganic and Organometallic Polymers*, **2**, 151 (1992).
17. F. Bauer, U. Decker, A. Dierdof, H. Ernst, R. Heller, H. Liebe and R. Mehnert, *Progress in Organic coating*, **53**, 183 (2005).
18. D. Bahloul, M. Pereira, P. Goursat, N.S. Choong Kwet Yive and R.J.P. Corriu, *Journal of American Ceramic Society*, **76**, 1156 (1993).
19. R.J.P. Corriu, *Angewandte Chemie International Edition in English*, **39**, 1376 (2000).
20. M. Landkof, A.V. Levy, D.H. Boone, R. Gray, E. Yaniv, *Corrosion-NACE* **41**, 344 (1985).
21. C.S. Tedmon, *Journal of Electrochemical Society* **113**, 766 (1966).
22. H.C. Graham and H.H. Davis, *American Ceramic Society Bulletin* **49**, 394 (1970).
23. K. Segerdahl, J.E. Svensson, L.G. Johansson, *Materials and Corrosion* **53**, 247 (2002).
24. H.E. Evans, A.T. Donaldson, T.C. Gilmour, *Oxidation of Metals* **52**, 379 (1999).
25. A. Galerie, S. Henry, Y. Wouters, J.P. Petit, L. Antoni, *Materials at High Temperature* **21**, 105 (2005).
26. M. Günthner, T. Kraus, A. Dierdorf, D. Decker, W. Krenkel, G. Motz, *Journal of the European Ceramic Society*, **29**, 2061 (2009).
27. F. Riffard, H. Buscail, E. Caudron, R. Cueff, C. Issartel, S. Perrier, *Materials Characterization* **49**, 55 (2002).
28. J. Xu, J. Favergeon, P.E. Mazeran, G. Moulin, C. Vu, *Materials Science Forum*, **696**, 308 (2011).
29. A. Schutz, M. Günthner, G. Motz, O Greißl, U. Glatzel, *Surface & CoatingsTechnology*, **207**, 319 (2012).
30. S. Traßl, D. Suttor, G. Motz, E. Rössler, G. Ziegler, *Journal of the European Ceramic Society*, **20**, 215 (2000).
31. M. Günthner, A. Schütz, U. Glatzel, K. Wang, R.K. Bordia, O. Greißl, W. Krenkel, G. Motz, *Journal of the European Ceramic Society*, 31**,** 3003 (2011).